

MIT Open Access Articles

*Externally Pumped Photonic Chip#
Based Ultrafast Raman Soliton Source*

The MIT Faculty has made this article openly available. **Please share** how this access benefits you. Your story matters.

Citation: Li, Zhao, Du, Qingyang, Wang, Chaopeng, Zou, Jinhai, Du, Tuanjie et al. 2020. "Externally Pumped Photonic Chip#Based Ultrafast Raman Soliton Source." *Laser & Photonics Reviews*, 15 (2).

As Published: <http://dx.doi.org/10.1002/lpor.202000301>

Publisher: Wiley

Persistent URL: <https://hdl.handle.net/1721.1/140936>

Version: Author's final manuscript: final author's manuscript post peer review, without publisher's formatting or copy editing

Terms of use: Creative Commons Attribution-Noncommercial-Share Alike



Externally pumped photonic chip-based ultrafast Raman soliton source

Zhao Li[†], Qingyang Du^{†,*}, Chaopeng Wang[†], Jinhai Zou, Tuanjie Du, Kathleen A. Richardson, Zhiping Cai, Juejun Hu, Zhengqian Luo^{*}

([†]These authors contributed equally to this work)

Z. Li, C. Wang, J. Zou, Dr. T. Du, Prof. Z. Cai, Prof. Z. Luo
Department of Electronic Engineering, Xiamen University, Xiamen, 361005, China
E-mail: zqluo@xmu.edu.cn

Dr. Q. Du, Prof. J. Hu
Department of Materials Science & Engineering, Massachusetts Institute of Technology, Cambridge, MA 02139, USA
E-mail: qydu@mit.edu

Prof. K. A. Richardson
The College of Optics & Photonics, Department of Materials Science & Engineering, University of Central Florida, Orlando, FL 32816, USA

Keywords: chalcogenide glass, Raman soliton self-frequency shift, ultrafast laser, nanophotonics

The advantages of low cost, compact size, and reduced power consumption makes a photonic chip-based ultrafast laser sources an appealing technology for diverse applications such as all-optical signal processing, frequency metrology, spectroscopy, and sensing. To date, on-chip ultrafast sources are typically generated by microresonator-based Kerr-comb solitons which require precise phase tuning and frequency agile lasers to access the soliton state. Here, our work reports the first experimental demonstration of externally pumped on-chip ultrafast soliton laser source based on Raman soliton self-frequency shift. By capitalizing on strong optical nonlinearity and versatile dispersion control in Ge₂₈Sb₁₂Se₆₀ chalcogenide glass waveguides, 185 fs duration Raman soliton generation was demonstrated, possessing continuous wavelength tunability from 1589 nm to 1807 nm with signal-to-noise ratios consistently exceeding 65 dB. The source operates with pump pulse energies as low as 1.08 pJ, representing over three orders of magnitude improvement compared to fiber-based Raman soliton sources. In addition, the generated solitons exhibit excellent spectral purity and stability free from parasitic sidebands. These experimental results are further validated by theoretical analysis, revealing insights into the soliton dynamics and critical device design guidelines. Our work therefore enables a new class of broadly tunable, energy-efficient, compact, and potentially cost-effective on-chip ultrafast laser sources.

1. Introduction

Ultrafast laser sources with sub-picosecond pulse duration and high peak power are widely deployed for applications covering material processing, optical ranging, frequency metrology, spectroscopy, and communications^[1-4]. Generation of ultrafast laser pulses has largely relied upon mode-locked lasers, and further coupled with nonlinear frequency conversion (e.g. second harmonic generation, parametric processes) to extend the operation wavelength range. Ultrafast lasers have been intensively investigated in bulk crystal or fiber platforms, enabling ultrashort pulse duration down to the few-fs regime and petawatt-class peak power. However, the bulky size, high cost and large power consumption of these sources can limit their potential applications in emerging areas exemplified by on-chip all-optical signal processing^[5] and spectroscopic sensing^[6].

Address(es) of author(s) should be given

Copyright line will be provided by the publisher

This is the author manuscript accepted for publication and has undergone full peer review but has not been through the copyediting, typesetting, pagination and proofreading process, which may lead to differences between this version and the Version of Record. Please cite this article as doi: 10.1002/lpor.202000301

Photonic chip-based ultrafast lasers offer a promising route to overcome the size, weight, power and cost (SWaP-C) limitations. To date, increasing numbers of works on photonic chip-based ultrafast lasers have been reported via on-chip laser mode-locking^[7,8] or microresonator Kerr combs^[9-15]. Shtyrkova et al. demonstrated an 1880 nm, 215 fs soliton source by growing a Tm³⁺-doped Al₂O₃ waveguide on SiN photonic chip platform^[7]. However, the fabrication is complex and only a small portion of the field is interacting with the gain material evanescently, sacrificing the pump efficiency. In addition, the rare-earth emission spectrum largely limited the soliton wavelength range. On the other hand, on-chip microresonator Kerr-comb solitons have been widely presented using different waveguide materials (e.g. SiN, silicon)^[9-17], but the implementation is quite demanding which usually requires frequency agile lasers and precise phase control. In contrast, Raman soliton self-frequency shift (SSFS), an intra-pulse scattering process, represents another useful mechanism for widely tunable solitons. Although SSFS in optical fibers has been well used for flexible-wavelength ultrashort pulse generation^[18-22], SSFS in on-chip waveguide platform has been not fully exploited yet. It worth mentioning that SSFS has been observed in dissipative Kerr solitons inside a resonant cavity in an on-chip platform^[17], however, the tuning range is merely ~ 20 nm, which is an order of magnitude smaller than conventional SSFS in a fiber and thus cannot be effectively implemented as a tunable source. Compared to those prevailing solutions for on-chip ultrafast pulse generation thus far, Raman SSFS features several unique advantages: 1) Most importantly, SSFS does not require precise phase tuning^[11], thereby eliminating the need for stringent phase lock control and temperature stabilization; 2) Raman SSFS mechanism naturally recreates itself to broadband and continuously spectral tunable ultrafast pulses, contributing to a high pump efficiency; 3) and therefore, the pump pulse energy for exciting Raman solitons is several orders of magnitude lower than those needed to produce other forms of on-chip solitons. These attractive features qualify Raman solitons as an ideal solution for extending new-wavelength on-chip ultrafast laser, as has been evidenced by prior theoretical analysis^[123].

In this paper, we report the first experimental demonstration of an on-chip ultrafast laser source based on Raman SSFS. By fully exploiting strong optical nonlinearity and broadband transparency of Ge₂₈Sb₁₂Se₆₀ chalcogenide glass waveguides, we have demonstrated 185 fs duration Raman soliton generation, continuously tunable over 200 nm spectral range from 1589 nm to 1807 nm. We emphasize that the Raman soliton starts operating with pump pulse energies as low as 1.08 pJ, which represents three orders of magnitude improvement compared to fiber-based Raman soliton sources^[18-21]. Our demonstrated low power consumption and compact soliton source prototype represents one of the last key components of realizing lab-on-a-chip IR systems for sensing as well as data communications applications.

2. Results

2.1. Experimental designs and setup

We chose chalcogenide glasses (ChGs) as the waveguiding material for SSFS. Compared with silicon based materials, ChGs large optical nonlinear coefficient (~ 900 times that of silica^[24]) warrants orders of magnitude reduction in requisite pump power. Moreover, the glass relatively low mechanical stiffness provides waveguiding for elastic waves in Brillouin and Raman scattering, significantly increasing the photon-phonon interaction length^[25]. ChGs are thus ideally poised for applications in on-chip nonlinear photonics benefitting from this unique dual confinement of both optical and elastic waves. On-chip devices for high-speed all-optical signal regeneration^[26], wavelength conversion^[27], and supercontinuum generation^[28] capitalizing on the nonlinear responses in ChGs have been recently demonstrated. Additionally, these glasses show broad compositional tunability to meet processing and performance metrics, and have been shown to be compatible with CMOS fabrication platforms, amenable to loss reduction methodologies and meet the design and fabrication criteria needed for multi-material compatibility requirements, necessary for on-chip device integration.^[29]

For the present effort, we specifically, chose low toxicity, Arsenic free Ge₂₈Sb₁₂Se₆₀ (GeSbSe)^[30-34] as the target ChG composition given its large linear and nonlinear indices ($n = 2.8$, $n_2 = 5.1 \times 10^{-18} \text{ m}^2\text{W}^{-1}$) and negligible two photon absorption at the telecom wavelength. GeSbSe waveguides were fabricated following previously established protocols (see Methods for details)^[35]. Waveguides with the same height of $0.4 \mu\text{m}$, varying widths from $0.8 \mu\text{m}$ to $1 \mu\text{m}$, and two different lengths (11.0 mm and 23.8 mm) were prepared. Micrographs of as-fabricated devices are shown in **Figure 1a**. To enhance fiber coupling efficiency, the waveguides are terminated with ChG inverse tapers embedded in an SU-8 epoxy waveguide (see Figure 1b-1c). Compared to direct cleaved ChG waveguide facets, the inverse-taper coupler structure increases the coupling efficiency by 3 dB/facet.

Since Raman SSFS is sensitive to the group velocity dispersion (GVD) of the waveguide, we plot the GVD curves of the fundamental quasi-TE mode with three waveguide widths in Figure 1d. At a central pump wavelength of $1.56 \mu\text{m}$, the GVD transitions from the anomalous to normal dispersion regime as the waveguide width increases from $0.8 \mu\text{m}$ to $1 \mu\text{m}$. To efficiently excite Raman SSFS while suppressing supercontinuum generation, the device must operate in the strongly anomalous dispersion regime. Therefore, we expect that waveguides with $0.8 \mu\text{m}$ width are optimal for Raman soliton generation, a conclusion supported by our experimental Raman SSFS measurement and numerical simulation in later.

The measurement was performed on a setup schematically illustrated in Figure 1f. We used a home-built ultra-compact ($12\text{ cm} \times 10\text{ cm} \times 5\text{ cm}$) mode-locked fiber laser as the pump source. The lasers temporal and spectral pulse shapes are provided in Figure 1e. The laser has a center wavelength of 1560 nm and emits 120 fs pulses, corresponding to a spectral bandwidth of $\sim 40\text{ nm}$. More details of the pump laser are furnished in Supplementary Materials. The laser light was coupled in and out the chip via tapered lensed fibers and a red reference laser was used to facilitate coupling (Figure 1g). Finally, the collected light was analyzed with optical and electrical analyzers.

2.2. Experimental results

The spectral evolution of Raman solitons in a $0.8\text{ }\mu\text{m}$ wide and 23.8 mm long waveguide is depicted in **Figure 2a**. As the pump pulse energy increases from 1.08 pJ to 14.32 pJ , the Raman soliton progressively red shifts its center frequency, enabling continuous tuning of the emission wavelength from 1589 nm to 1807 nm . The waveguide's anomalous dispersion peaks at $1.82\text{ }\mu\text{m}$ wavelength [see Figure 1(d)], which prevents SSFS beyond this wavelength and dictates the upper limit of the tuning range. As pump pulse energy increases, the Raman soliton generation efficiency, defined as the energy ratio of the Raman soliton pulse to the total pulse energy, improves from 32% to 61%. We observed SSFS onset at pump pulse energies as low as 1.08 pJ , significantly lower than that seen in a high nonlinear fiber (HNLF)^[36] (nJ power) and in an on-chip dissipative Kerr soliton source^[13] ($\sim 100\text{ mW}$ CW pump power). This remarkably low power consumption makes the technology particularly appealing for applications such as spectroscopy, metrology, as well as optical signal processing and computing.

We then investigated the impact of waveguide geometry on SSFS. Shown in Figure 2b is the comparison of Raman soliton spectra generated with 11.0 mm and 23.8 mm long waveguides at two different pump levels. We find that the waveguide length hardly affects the SSFS wavelength, although longer waveguide leads to better pump pulse-to-soliton conversion efficiency. Figure 2c presents the soliton spectra generated by waveguides of different widths. For the $0.8\text{ }\mu\text{m}$ wide waveguide, a Raman soliton can be clearly identified at a center wavelength of 1640 nm , whereas the $0.9\text{ }\mu\text{m}$ wide waveguide generates a broad supercontinuum spanning half an octave resulting from pumping near the zero-dispersion wavelength (ZDW). The $1.0\text{ }\mu\text{m}$ wide waveguide similarly produces a supercontinuum albeit with narrower bandwidth due to pumping at the normal dispersion regime. The results are consistent with our GVD simulations (Figure 1d) and define the distinct regimes favoring Raman soliton and supercontinuum generation respectively.

The temporal characteristics of the Raman soliton were also studied. We focused on the soliton generated with a pump pulse energy of 7.73 pJ . Pure Raman soliton were obtained after filtering the pump pulse with a fiber end-facet dielectric mirror filter, and the resulting spectrum is displayed in **Figure 3a**. This soliton centers at 1748 nm and has a full-width at half-maximum (FWHM) of 41 nm . Figure 3b shows the temporal profile of a soliton pulse train recorded by an oscilloscope. The pulses exhibit a period of 70 ns , same as that of the pump source. Notably, the pulse train is free of parasitic sidebands, confirming high purity and stability of the Raman solitons. The autocorrelation trace of a typical single pulse is plotted in Figure 3c. A sech^2 fit yields a pulse temporal FWHM of 185 fs , corresponding to a time-bandwidth product of 0.74 . The product is about twice larger than that in a bandwidth-limited pulse (0.315), indicating that the solitons are slightly chirped. The chirp is found to originate from amplification of the pump pulse (see Supplementary Materials) and can be eliminated by optimizing the 1560 nm femtosecond pump source. Figure 3d gives the output radio-frequency spectrum of the Raman soliton train. The fundamental repetition rate is 14.298 MHz with a signal-to-noise ratio (SNR) of 65 dB . The high SNR figure is comparable to state-of-art fiber mode-locked lasers^[37-39] and on-chip soliton sources^[14]. It is also interesting to note that there is almost no frequency-dependent modulation of the pulse intensity within a 3 GHz frequency span, evidenced by the broadband radio-frequency spectrum shown in Figure 3d inset. The results demonstrate exceptional stability and high quality of the Raman solitons.

2.3. Numerical simulations

Further insight into the on-chip Raman SSFS kinetics is provided by numerically solving the generalized nonlinear Schrodinger equation (GNLSE). Details of the simulation parameters can be found in Supplementary Materials. **Figures 4a** and **4b** plot the spectral and temporal evolution of a 120 fs , 4.92 pJ pumped Raman soliton in a $0.4\text{ }\mu\text{m} \times 0.8\text{ }\mu\text{m}$ waveguide. When the pump pulse is injected into the waveguide, initial spectral broadening occurs via self-phase modulation. Beyond the critical length of 3.2 mm , SSFS becomes the dominant effect, red shifting the center wavelength to $\sim 1780\text{ nm}$. In the meantime, a dispersive wave is generated in the shorter wavelength regime ($\sim 1100\text{ nm}$) to conserve the total momentum. As the pulse propagates further, the pump-to-soliton conversion efficiency continues to increase while the soliton center wavelength remains constant. This result agrees with our finding in Figure 2b that above the critical length, waveguide length does not affect the SSFS wavelength. In the time domain, once the critical length is reached, the pump pulse rapidly dissociates and a stable branch corresponding to the propagation trace of the Raman soliton is formed, accompanied with a fast decaying dispersive wave branch.

The effect of pump pulse energy on Raman SSFS was also investigated in the simulation. The spectral and temporal domain simulation results are displayed in Figure 4c and 4d for a 23.8 mm long waveguide. Formation of the Raman soliton is apparent even at a very low pump pulse power of 1.08 pJ; though spectrally merged to the pump pulse (Figure 4c), a distinct sech^2 pulse with positive time delay can be clearly identified, a unique signature indicating Raman soliton formation. This pump energy in the simulation matches with our experimental value at the onset, but becomes increasingly underestimated as we move to higher pulse energy. This phenomenon is primarily due to nonlinear chirp of our pump pulse introduced during amplification of the seed laser. The chirping effect reduces peak power of the pump pulse, resulting in a higher average power to realize the same SSFS. In addition to the exceptionally low power requirement, the simulation results also reproduce the Raman soliton generation process as free of parasitic sidebands in both spectral and temporal domains, in agreement with our experimental measurement. The simulated individual soliton pulse characteristics are given in Figure 4e. Compared with our measured results in Figure 3, the simulated pulse FWHMs are smaller in both spectral and temporal domains, which is also attributed to pulse chirping. Finally, we validated the Raman soliton generation efficiency in different waveguide geometries (Figure 4f). The simulations match well with our experimental results in Figure 2c. It is worth further noting that even though anomalous dispersion is even larger with a smaller waveguide width of 0.6 μm , the dispersion broadens the pulse and diminishes its peak power before reaching the critical length. Consequently, Raman SSFS is suppressed. This result therefore suggests that 0.8 μm is indeed the optimum waveguide width for Raman soliton generation given the waveguide material and height.

3. Conclusion

In summary, we have demonstrated a compact ultrafast soliton source leveraging Raman SFSS on a ChG photonic chip. The source is continuously tunable between 1560 nm to 1807 nm, and boasts an ultra-low onset pump energy in the low picojoule range. Numerical simulations confirm that the pump energy can be further reduced using a chirpless and shorter-duration soliton source. Our work opens up a practical route toward a miniaturized fiber packaged, compact photonic chip-scale platform for ultrafast optics with broad applications in all-optical signal processing, spectroscopy, optical ranging, and sensing.

4. Experimental Section/Methods

A schematic drawing of the fabrication process is provided in Figure S1. WaferPro Si wafer substrates with 3 μm thermally grown oxide were piranha cleaned to remove organic residues. Immediately after, GeSbSe bulk glass, produced using standard melt-quench protocols for use as target media for planar structures^[40] was thermally evaporated onto the wafer to form a 400 nm thick thin film following standard protocols^[41]. During subsequent lithographic processing, an electron beam resist ZEP 520A (Zion chemicals) was spun onto the sample and then exposed on an Elionix F-125 electron beam lithography (EBL) tool with a beam current of 10 nA. The chip was then developed with ZED-N50 (Zion chemicals) developer to reveal the waveguide pattern. GeSbSe glass was then etched in a PlasmaTherm reactive ion etcher with a gas mixture of $\text{CHF}_3:\text{CF}_4 = 3:1$ at 200 W RF power. After the etch was completed, the chip was immersed in N-Methyl-2-Pyrrolidone (NMP) solution overnight to remove remaining ZEP and etching polymer residues. To enhance fiber-to-chip coupling efficiency, SU-8 encapsulated inverse tapers were added to the coupler. SU-8 2002 (Microchem) was spun on to the as-fabricated chip and then exposed with the same EBL tool. The process was completed after developing the chip in 1-Methoxy-2-propyl acetate (PMEGA).

Supporting Information

Supporting Information is available from the Wiley Online Library or from the author.

Acknowledgement

This work is funded by National Science Foundation (NSF) (1506605). National Natural Science Foundation of China (NSFC) (61475129); Fundamental Research Funds for the Central Universities (20720180057); Natural Science Foundation of Fujian Province for Distinguished Young Scientist (2017J06016); Program for the Young Top Notch Talents of Fujian Province; Program for the Nanqiang Young Top Notch Talents of Xiamen University. We sincerely thank Dr. Yizhong Huang from University of Chicago for insightful discussion about the manuscript.

Conflict of Interest

The authors declare no conflict of interest.

Received: ((will be filled in by the editorial staff))

Received: ((will be filled in by the editorial staff))

Received: ((will be filled in by the editorial staff))

References

- [1] M. Malinauskas, A. ukauskas, S. Hasegawa, Y. Hayasaki, V. Mizeikis, R. Buividas, S. Juodkazis, *Light-Sci. Appl.* **2016**, *5*, e16133.
- [2] P. Trocha, M. Karpov, D. Ganin, M. H. Pfeiffer, A. Kordts, S. Wolf, J. Krockenberger, P. Marin-Palomo, C. Weimann, S. Randel, *Science* **2018**, *359*, 887.
- [3] T. Udem, R. Holzwarth, T. W. Hensch, *Nature* **2002**, *416*, 233.
- [4] M. E. Fermann, I. Hartl, *Nat. Photonics* **2013**, *7*, 868.
- [5] C. Koos, P. Vorreau, T. Vallaitis, P. Dumon, W. Bogaerts, R. Baets, B. Esembeson, I. Biaggio, T. Michinobu, F. Diederich, *Nat. Photonics* **2009**, *3*, 216.
- [6] D. Dai, *Opt. Express* **2009**, *17*, 23817.
- [7] K. Shtyrkova, P. T. Callahan, N. Li, E. S. Magden, A. Ruocco, D. Vermeulen, F. X. Krtner, M. R. Watts, E. P. Ippen, *Opt. Express* **2019**, *27*, 3542.
- [8] C. Grivas, R. Ismaeel, C. Corbari, C. C. Huang, D.W. Hewak, P. Lagoudakis, *Laser Photonics Rev.* **2018**, *12*, 1800167.
- [9] V. Brasch, M. Geiselmann, T. Herr, G. Lihachev, M. H. Pfeiffer, M. L. Gorodetsky, T. J. Kippenberg, *Science* **2016**, *351*, 357.
- [10] V. Brasch, E. Lucas, J. D. Jost, M. Geiselmann, T. J. Kippenberg, *Light-Sci. Appl.* **2017**, *6*, e16202.
- [11] Q. Li, T. C. Briles, D. A. Westly, T. E. Drake, J. R. Stone, B. R. Ilic, S. A. Diddams, S. B. Papp, K. Srinivasan, *Optica* **2017**, *4*, 193.
- [12] J. Liu, A. S. Raja, M. Karpov, B. Ghadiani, M. H. Pfeiffer, B. Du, N. J. Engelsen, H. Guo, M. Zervas, T. J. Kippenberg, *Optica* **2018**, *5*, 1347.
- [13] M. H. Pfeiffer, C. Herkommer, J. Liu, H. Guo, M. Karpov, E. Lucas, M. Zervas, T. J. Kippenberg, *Optica* **2017**, *4*, 684.
- [14] M. G. Suh, Q. F. Yang, K. Y. Yang, X. Yi, K. J. Vahala, *Science* **2016**, *354*, 600.
- [15] Q. F. Yang, X. Yi, K. Y. Yang, K. Vahala, *Nat. Phys.* **2017**, *13*, 53.
- [16] F. M. Mitschke, L. F. Mollenauer, *Opt. Lett.* **1986**, *11*, 659.
- [17] A. L. Gaeta, M. Lipson, T. J. Kippenberg, *Nat. Photonics* **2019**, *13*, 158.
- [18] X. Liu, C. Xu, W. H. Knox, J. K. Chandalia, B. J. Eggleton, S. G. Kosinski, R. S. Windeler, *Opt. Lett.* **2001**, *26*, 358.
- [19] T. Cheng, Y. Kanou, K. Asano, D. Deng, M. Liao, M. Matsumoto, T. Misumi, T. Suzuki, Y. Ohishi, *Appl. Phys. Lett.* **2014**, *104*, 121911.
- [20] M. Y. Koptev, E. A. Anashkina, A. V. Andrianov, V. V. Dorofeev, A. F. Kosolapov, S. V. Muravyev, A. V Kim, *Opt. Lett.* **2015**, *40*, 4094.
- [21] Y. Tang, L. G. Wright, K. Charan, T. Wang, C. Xu, F. W. Wise, *Optica* **2016**, *3*, 948.
- [22] M. Karpov, H. Guo, A. Kordts, V. Brasch, M. H.P. Pfeiffer, M. Zervas, M. Geiselmann, T. J. Kippenberg, *Phys. Rev. Lett.* **2016**, *116*, 103902.
- [23] A. C. Judge, S. A. Dekker, R. Pant, C. M. d. Sterke, B. J. Eggleton, *Opt. Express* **2010**, *18*, 14960.
- [24] J. T. Gopinath, M. Soljai, E. P. Ippen, V. N. Fufluyigin, W. A. King, M. Shurgalin, *J. Appl. Phys.* **2004**, *968*, 6931.
- [25] B. J. Eggleton, C. G. Poulton, P. T. Rakich, M. J. Steel, G. Bahl, *Nat. Photonics* **2019**, *13*, 664.
- [26] S. J. Madden, D. Y. Choi, D. A. Bulla, A. V. Rode, B. Luther-Davies, V. G. Taeed, M. D. Pelusi, B. J. Eggleton, *Opt. Express* **2007**, *15*, 14414.
- [27] M. Pelusi, F. Luan, S. Madden, D.-Y. Choi, D. Bulla, B. Luther-Davies, B. J. Eggleton, *IEEE Photonic. Tech. L.* **2009**, *22*, 3.
- [28] Q. Du, Z. Luo, H. Zhong, Y. Zhang, Y. Huang, T. Du, W. Zhang, T. Gu, J. Hu, *Photonics Res.* **2018**, *6*, 506.
- [29] Y. Zhang, J. B. Chou, J. Li, H. Li, Q. Du, A. Yadav, S. Zhou, M. Y. Shalaginov, Z. Fang, H. Zhong, *Nat. Commun.* **2019**, *10*, 1.
- [30] Y. Zou, L. Moreel, L. Savelli, H. Lin, J. Zhou, L. Li, S. Danto, J. D. Musgraves, K. Richardson, K. Dobson, R. Birkmire, J. Hu, *Adv. Opt. Mater.* **2014**, *2*, 759.
- [31] S. Serna, H. Lin, C. Alonso-Ramos, A. Yadav, X. L. Roux, K. Richardson, E. Cassan, N. Dubreuil, J. Hu, L. Vivien, *Photonics Res.* **2018**, *6*, B37.
- [32] T. Kuriakose, E. Baudet, T. Halenkovi, M. M. R. Elsayy, P. Nmec, V. Nazabal, G. Renversez, M. Chauvet, *Opt. Commun.* **2017**, *403*, 352.
- [33] T. Cardinal, K. A. Richardson, H. Shim, A. Schulte, R. Beatty, K. L. Foulgoc, C. Meneghini, J. F. Viens, A. Villeneuve, *J. Non-Cryst. Solids* **1999**, *256*, 353.
- [34] B. J. Eggleton, T. D. Vo, R. Pant, J. Schr, M. D. Pelusi, D. Y. Choi, S. J. Madden, B. Luther-Davies, *Laser Photonics Rev.* **2012**, *6*, 97.
- [35] Q. Du, Y. Huang, J. Li, D. Kita, J. Michon, H. Lin, L. Li, S. Novak, K. Richardson, W. Zhang, *Opt. Lett.* **2016**, *41*, 3090.
- [36] J. H. Lee, J. van Howe, C. Xu, X. Liu, *IEEE J. Sel. Top. Quant.* **2008**, *14*, 713.
- [37] B. Guo, S. H. Wang, Z. X. Wu, Z. X. Wang, D. H. Wang, H. Huang, F. Zhang, Y. Q. Ge, H. Zhang, *Opt. Express* **2018**, *26*, 22750.

- [38] M. Zhang, E. J. R. Kelleher, T. H. Runcorn, V. M. Mashinsky, O. I. Medvedkov, E. M. Dianov, D. Popa, S. Milana, T. Hasan, Z. Sun, F. Bonaccorso, Z. Jiang, E. Flahaut, B. H. Chapman, A. C. Ferrari, S. V. Popov, J. R. Taylor, *Opt. Express* **2013**, *21*, 23261.
- [39] D. Mao, S. Zhang, Y. Wang, X. Gan, W. Zhang, T. Mei, Y. Wang, Y. Wang, H. Zeng, J. Zhao, *Opt. Express* **2015**, *23*, 27509.
- [40] K. Richardson, L. Petit, N. Carlie, B. Zdyrko, I. Luzinov, J. Hu, A. Agarwal, L. Kimerling, T. Anderson, M. Richardson, *J. Nonlinear Opt. Phys.* **2010**, *19*, 75.
- [41] J. Hu, V. Tarasov, A. Agarwal, L. Kimerling, N. Carlie, L. Petit, K. Richardson, *Opt. Express* **2007**, *15*, 2307.

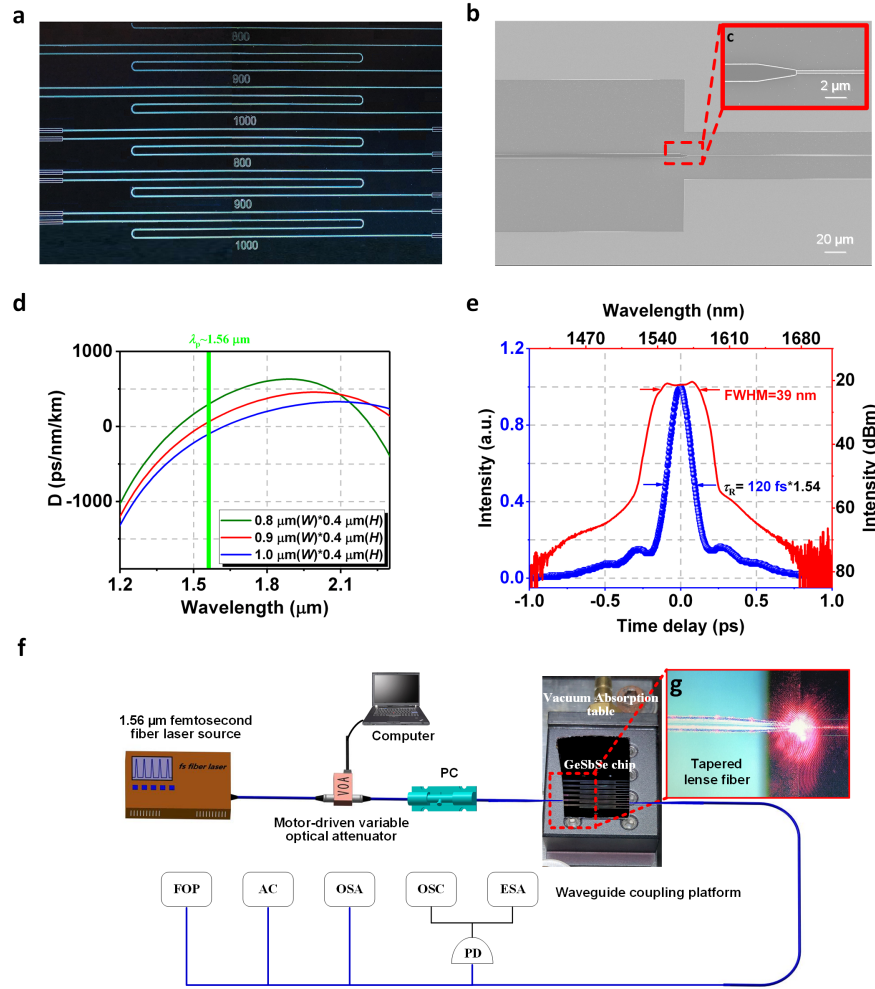


Figure 1 (a) Optical microscope image of an as-fabricated device with varying waveguide width between 800 nm to 1000 nm as labeled on the chip. The SU8 coupler sections are visible to the right. (b, c) SEM top views of the inverse taper, where light adiabatically transfers from the GeSbSe core (right) to an SU-8 core (left). (d) group velocity dispersion corresponding to the three different waveguide widths; the pump laser wavelength is marked with the green line. (e) spectral and temporal pulse shapes of the pump pulse laser. (f) a schematic drawing of experimental setup (PC: Polarization controller, AC: Autocorrelator, OSA: Optical spectrum analyzer, OSC: Oscilloscope, ESA: Electrical spectrum analyzer, and PD: photodetector). (g) optical microscope image showing red-light-aided fiber-to-chip coupling.

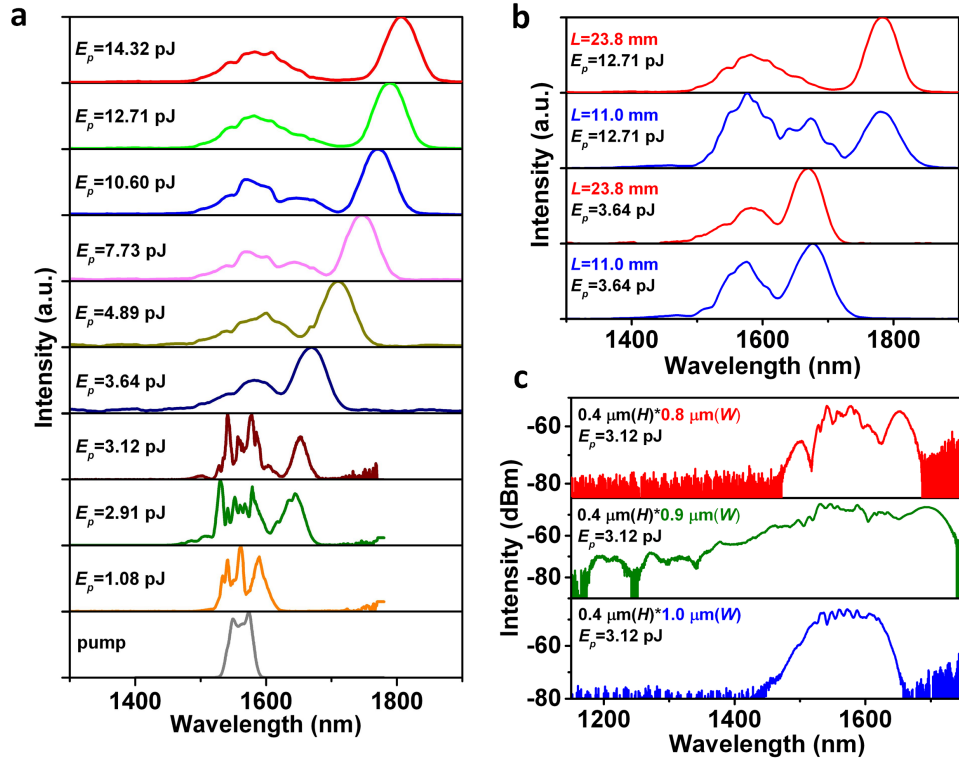


Figure 2 Spectral evolution of on-chip Raman solitons. (a) Spectral evolution of Raman solitons generated in a $400 \text{ nm (H)} \times 800 \text{ nm (W)} \times 23.8 \text{ mm (L)}$ waveguide with increasing pump pulse energy. The output spectra below $E_p = 7.49 \text{ pJ}$ were recorded with an ANDO AQ6317B OSA and the rest were recorded with an Ocean Optics OSA (NIRQuest512-2.5). (b) Raman soliton spectra with two different waveguide lengths and at two different pump power levels. (c) Output spectra from different waveguide cross-sectional geometries under the same pump energy level.

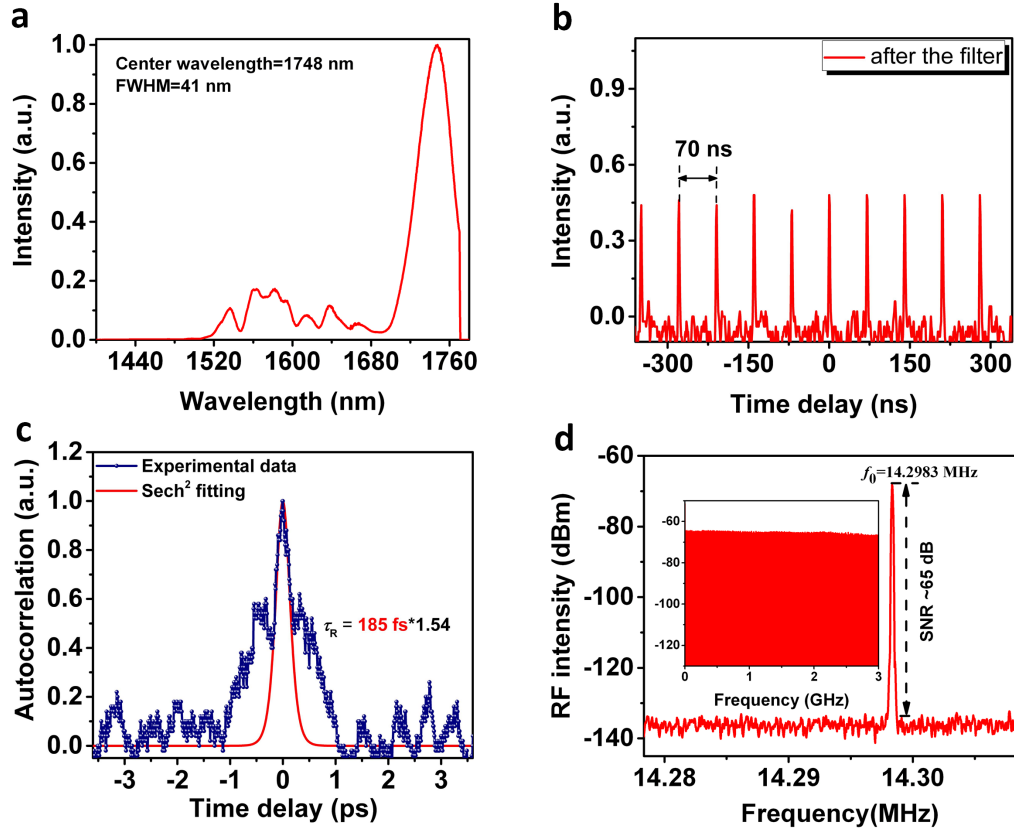


Figure 3 Temporal characteristics of on-chip Raman solitons. (a) Raman soliton spectrum under 7.73 pJ pump pulse energy filtered by a fiber end-facet dielectric mirror filter. It has a center wavelength of 1748 nm and a 41 nm FWHM. (b) Raman soliton pulse train after the filter. The period is 70 ns. (c) Autocorrelation trace of the Raman soliton, where a sech^2 curve is used to fit the curve yielding a bandwidth of 185 fs. (d) frequency domain analysis of the Raman soliton indicating a repetition rate of 14.2983 MHz and a high SNR of 65 dB. The bandwidth resolution is 10 Hz. The inset shows a broadband radio-frequency spectrum of Raman pulse train, where the flat top characteristic of such pulse train suggests excellent soliton stability.

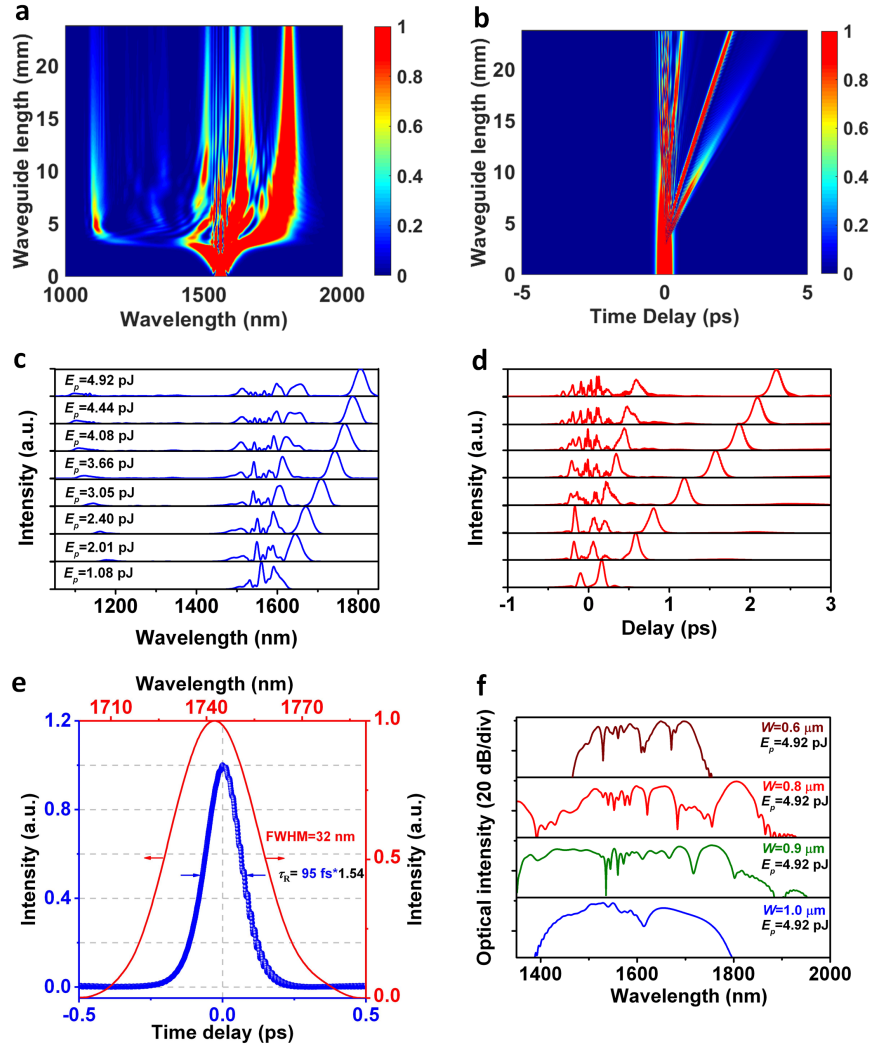


Figure 4 Numerical simulation of on-chip Raman solitons pumped with a 120 fs, 1.56 μm soliton pulse. (a) Spectral evolution and (b) temporal evolution results along the 23.8 mm waveguide. The pump energy is 4.92 pJ. The Raman soliton starts to form at a critical length of 3.2 mm. (c) Spectral and (d) temporal evolution of the Raman soliton as the pump pulse energy grows from 1.08 pJ to 4.92 pJ. (e) Simulated Raman soliton pulse characteristics. The FWHM is 32 nm with a 95-fs bandwidth. The discrepancy with our experiment demonstration is primarily due to nonlinear chirp of the pump laser pulse. (f) Spectra generated from the same pulse in various waveguide geometries. A distinct Raman pulse is found when $W = 0.8 \mu\text{m}$, whereas supercontinuum is observed in $0.9 \mu\text{m}$ and $1.0 \mu\text{m}$ wide waveguides. The large dispersion in $0.6 \mu\text{m}$ wide waveguide precludes SSFS at the pump energy level.